Photoelectron Imaging of Cyanovinylidene and Cyanoacetylene Anions

ARTICLE *in* THE JOURNAL OF PHYSICAL CHEMISTRY A · FEBRUARY 2010

Impact Factor: 2.69 · DOI: 10.1021/jp9106102 · Source: PubMed

3 AUTHORS, INCLUDING:

Dmitry Khuseynov
The University of Arizona
16 PUBLICATIONS **76** CITATIONS
SEE PROFILE

Andrei Sanov
The University of Arizona
103 PUBLICATIONS **1,450** CITATIONS
SEE PROFILE

Photoelectron Imaging of Cyanovinylidene and Cyanoacetylene Anions

Daniel J. Goebbert, Dmitry Khuseynov, and Andrei Sanov*

Department of Chemistry, University of Arizona, Tucson, Arizona 85721-0041

Received: November 6, 2009; Revised Manuscript Received: December 18, 2009

Negative ions of cyanoacetylene and cyanovinylidene are generated simultaneously via the competing 1,1-H_2^+ and 1,2-H_2^+ abstraction channels of O^- reaction with acrylonitrile. The two stable isomeric forms of the anion, $CCHCN^-$ and $HCCCN^-$, are separated by a large (~2 eV) potential energy barrier. Their photodetachment provides access to both the reactant and the product sides of the neutral cyanovinylidene → cyanoacetylene rearrangement reaction, predicted to involve only a very small barrier. Using photoelectron imaging spectroscopy at 532 and 355 nm, the adiabatic electron affinity of the reactive intermediate :C═CHCN (X^1A'), is determined to be 1.84 ± 0.01 eV. The photoelectron spectrum of $CCHCN^-$ exhibits a vibrational progression attributed to the excitation of the CCH bending mode. The observed spectral features are reproduced reasonably well using a Franck−Condon simulation under the parallel-mode approximation. In contrast to unsubstituted acetylene, cyanoacetylene has a stable anionic state, which is adiabatically weakly bound, but has an experimentally determined vertical detachment energy of 1.04 ± 0.05 eV. This measurement, along with the broad, structureless photoelectron spectrum of $HCCCN^-$ (with no identifiable origin), reflects the large geometry difference between the w-shaped structure of the anion and the linear equilibrium geometry of HCCCN.

1. Introduction

Photoelectron spectroscopy of negative ions has been used extensively to study reactive intermediates that shape the composition of our planet and the Universe. A classic example is the chemistry of vinylidene, :C═CH_2, which undergoes a rapid 1,2-hydrogen atom shift to the more stable acetylene structure, HC≡CH, with only a small (2 ± 1 kcal/mol) potential barrier.[1−7] In contrast to the neutral, the ground state of the $C_2H_2^-$ anion corresponds to the vinylidene geometry, CCH_2^-, while the acetylene anion, $HCCH^-$, is unstable. Thus, photodetachment of $C_2H_2^-$ provides access to the reactive (vinylidene) part of the neutral potential energy surface, where the CCH_2 → HCCH rearrangement ensues on a time scale ≤0.2 ps.[1,2]

In the present work, we use negative-ion photoelectron imaging to examine cyano-substituted vinylidene and acetylene, :C═CHCN and HC≡CCN, respectively. The relative energetics of the two neutral structures are qualitatively similar to those of vinylidene and acetylene, and so one might expect the behavior of cyanovinylidene to be comparable to that of vinylidene. Namely, CCHCN is expected to undergo rearrangement to the more stable HCCCN structure, with only a small (2.2 kcal/mol) barrier predicted by calculations.[8] Small rearrangement barriers are also found for other substituted vinylidenes, such as fluoro-, *tert*-butyl-, and vinylvinylidenes, which have been studied by both photoelectron spectroscopy[9−11] and theory.[12,13] Qualitative analysis suggests that the properties of cyanovinylidene should be similar to those of fluorovinylidene, since the CN substituent acts as a pseudohalogen. On the other hand, the conjugated π system with the CN substituent might also result in similarities to vinylvinylidene.

Due to the electron affinity of the CN group, the cyanovinylidene and cyanoacetylene anion structures are affected by the substitution to a greater extent than the corresponding neutrals. In stark contrast to acetylene, the cyanoacetylene anion, $HCCCN^-$, is in fact a stable species.[14,15] The large dipole moment and the unsaturated π system of HCCCN are responsible for the predicted existence of dipole-bound and valence anionic states.[14] These states have attracted attention not only because of their exotic fundamental properties, including the possible coupling between the dipole-bound and valence states of the anion,[14] but also because of the dissociative electron attachment to cyanoacetylene (involving these states) that may play a role in the formation of carbon-rich and CN-containing negative ions in extraterrestrial environments.[15−20] However, until recently[15] $HCCCN^-$ had eluded definitive experimental detection—not only in space but also in the laboratory. Despite the general interest in reactive intermediates, cyanovinylidene has also not been studied by anion photoelectron spectroscopy.

We demonstrate the simultaneous formation of $CCHCN^-$ and $HCCCN^-$, providing access (via photodetachment) to both the cyanovinylidene and cyanoacetylene sides of the CCHCN → HCCCN rearrangement reaction. The two isomeric forms of the anion are generated via the competing channels of O^- reaction with acrylonitrile, H_2C═CHCN. The vinylidene form of the anion is formed via the 1,1-H_2^+ abstraction pathway, while the valence anions of cyanoacetylene are formed via the *cis*- and/or *trans*-1,2-H_2^+ abstraction channel(s).[15]

The cyanovinylidene anion was indicated in a previous study of the reaction of O^- with 2-deuterioacrylonitrile (H_2C═CDCN),[21] but no evidence for the simultaneous formation of the cyanoacetylene anion had been reported. However, $HCCCN^-$ was once proposed in electron attachment to acrylonitrile, but that assignment has also not been confirmed.[22] The key to the formation of the elusive anion of $HCCCN^-$ in the present work is the bent $-\dot{C}$═$\dot{C}$—C≡ skeleton of the reactant acrylonitrile, contrasting the corresponding linear arrangement in neutral HCCCN.[15] High-level ab initio calculations by Sommerfeld and Knecht predicted a roughly w-shaped equilibrium geometry of valence $HCCCN^-$, which is adiabatically stable with respect to electron detachment by only 50 meV.[14]

* Corresponding author. E-mail: sanov@u.arizona.edu.

10.1021/jp9106102
Published on Web 01/21/2010

However, the large geometry difference between $HCCCN^-$ and HCCCN results in a sizable vertical detachment energy (VDE) of the anion, VDE = 1.04 eV, as determined by photoelectron spectroscopy.[15] This experimental determination is compared to the theoretical prediction of 1.25 eV.[14]

In this work, we characterize the stable valence anions of cyanovinylidene and cyanoacetylene by means of photoelectron imaging spectroscopy at 532 and 355 nm. The two anion isomers exhibit drastically different photoelectron spectra: a broad, unstructured band with no identifiable origin for $HCCCN^-$ and a resolved vibrational progression assigned to $CCHCN^-$. We examine the energetics of the two anion species revealed by their photoelectron spectra and model the vibrational progression in $CCHCN^-$ using a Franck−Condon simulation based on the parallel-mode approximation and the Duschinsky algorithm.[23]

2. Experimental Arrangement

The experiments were performed using a pulsed time-of-flight mass spectrometer with a velocity-map imaging detector that has been described previously.[24] Anions were generated by the reaction of O^- with acrylonitrile.[21,25] Acrylonitrile vapor was entrained in neat N_2O carrier gas with a backing pressure of 20 psi and expanded into high vacuum through a pulsed supersonic nozzle (General Valve, Inc., series 99) operating at a 50 Hz repetition rate. The expanding gas was crossed with a 1 keV electron beam, which produced slow secondary electrons by collisions with the neutral gas molecules. Dissociative electron attachment to N_2O generated O^-, which in turn reacted with acrylonitrile via the 1,1- or 1,2-H_2^+ abstraction channels to form the cyanovinylidene and cyanoacetylene anions, respectively.[15]

Thus formed negatively charged ions were extracted into a pulsed time-of-flight mass spectrometer and after acceleration to 3 keV entered a field-free region of the instrument, where the mass-selected $m/z = 51$ ions were irradiated with a linearly polarized output of a Nd:YAG laser (Spectra Physics, Inc., model Lab-50). The laser output was frequency doubled or tripled to produce 532 or 355 nm pulses, with a pulse width of ~8 ns and pulse energies of 30 and 10 mJ, respectively. Static electric fields within a velocity-map[26] imaging[27] assembly projected the photodetached electrons onto a position sensitive detector, and the resulting images were captured with a 1 megapixel camera. In all measurements, the laser polarization axis was set parallel to the detector plane. A typical data set included $\sim 10^5$ experimental cycles. The final images reported here are the compositions of three to four such data sets.

The nascent three-dimensional photoelectron distributions, which are cylindrically symmetric with respect to the laser polarization axis (z), were reconstructed from the photoelectron images using the inverse Abel transformation implemented in the BASEX program.[28] The electron kinetic energy (eKE) scale was calibrated using the known detachment energy of O^-.[29] The photoelectron spectra were obtained by integrating Abel-inverted photoelectron images with respect to the angular coordinate, while integration over a radial range yielded the photoelectron angular distributions (PADs) for the corresponding transitions. The PADs were analyzed to determine the values of the photoelectron anisotropy parameter β, which uniquely describes the angular distribution in a one-photon photodetachment transition.[30,31]

3. Electronic Structure and Franck−Condon Simulations

Electronic structure calculations were carried out at the B3LYP/aug-cc-pVDZ, MP2/aug-cc-pVDZ, and CCSD(T)/6-311++G** levels of theory using the Gaussian 03 program package.[32] The geometries for the anion and neutral ground and excited states were optimized with normal-mode analysis to confirm the structures corresponded to true potential minima. The energies of the neutral ground and excited states were also calculated at the optimized anion geometry to obtain estimates of the vertical detachment energies.

To simulate photoelectron spectra from the results of ab initio or density-functional theory calculations, we developed a program for calculating Franck−Condon factors of polyatomic molecules, which adopts the general procedure described by Duschinsky.[23] In this approach, the normal modes for the anion are expressed in generalized coordinates $\mathbf{Q}'$, while the coordinates for the neutral are expressed as $\mathbf{Q}$. The two sets of coordinates are related by the Duschinsky rotation matrix $\mathbf{J}$ and a displacement vector $\mathbf{K}$:[23]

$$\mathbf{Q}' = \mathbf{J}\cdot\mathbf{Q} + \mathbf{K} \tag{1}$$

We calculate $\mathbf{J}$ and $\mathbf{K}$ from normal coordinates and geometries using the methods outlined by Chen and co-workers[33] for converting Gaussian output from Cartesian coordinates to the generalized coordinates in a home-written LabView program. Evaluation of the multidimensional overlap integrals is a well-known, but generally complicated, problem.[33,34] We simplify it by making the parallel mode approximation, where $\mathbf{J}$ is set equal to the identity matrix $\mathbf{I}$. The Franck−Condon factors then simplify to a set of one-dimensional integrals:[35]

$$\langle \upsilon_1'\upsilon_2'\upsilon_3'...\upsilon_n'|\upsilon_1''\upsilon_2''\upsilon_3''...\upsilon_n''\rangle^2 = \prod_{i=1}^{n}\langle \upsilon_i'|\upsilon_i''\rangle^2 \tag{2}$$

where v_i' and v_i'' are the numbers of excitation quanta in mode i of the neutral and anion, respectively. The main advantage of the parallel mode approximation, compared to evaluation of the multidimensional overlap integrals, is realized when one considers combination bands. Using the parallel mode approximation, these integrals reduce to products of the one-dimensional overlap integrals.[35] Assuming all vibrations to be harmonic, we evaluate the integrals in eq 2 numerically for an arbitrary number of vibrational modes n.

Since the $\mathbf{J}$ matrix is approximately unitary, multiplying both sides of eq 1 by $\mathbf{J}^\mathbf{T}$ yields $\mathbf{J}^\mathbf{T}\mathbf{J} \approx \mathbf{I}$. Similarly, $\mathbf{J}^\mathbf{T}\mathbf{K} = \mathbf{K}'$, where $\mathbf{K}'$ is a set of effective displacement vectors weighted by the magnitude of the diagonal matrix elements J_{ii}. The vibrational modes of the anion and neutral do not necessarily follow the same ordering, and multiple modes of the anion may match a single mode of the neutral (and vice versa), leaving the remaining modes unassigned.[35] We manually assign the vibrational modes to maximize the overlap of the two states, which guarantees the best description within the parallel mode approximation.

The validity of the parallel mode approximation is verified by inspecting the Duschinsky matrix, $\mathbf{J}$. The matrix describes the extent of mixing between vibrational modes of the same symmetry between two or more states, where off-diagonal elements indicate the extent to which different states mix.[33,34] If the diagonal elements are all close to 1, the parallel mode approximation is valid, whereas if any diagonal element is significantly less than 1, the full multidimensional calculation may be required. In our simulations of the photoelectron spectrum of $CCHCN^-$, the diagonal elements were close to 1, indicating that the parallel mode approximation is reasonable for this system. The approximation's validity is due to the similar

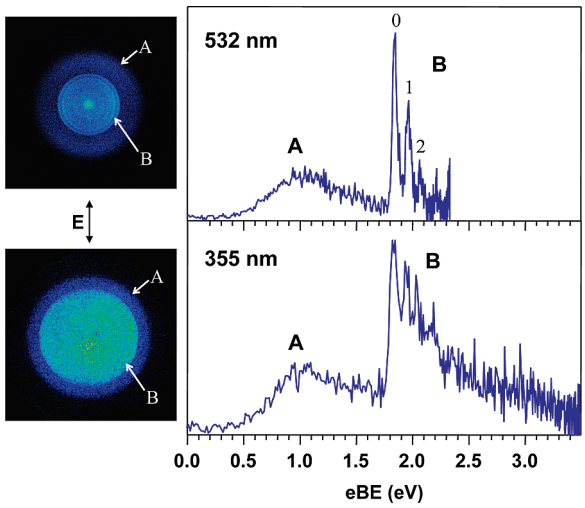

Figure 1. Photoelectron images and spectra of $HCCCN^-$ and $CCHCN^-$ obtained at 532 and 355 nm. The laser polarization axis is vertical in the plane of the images. Bands A and B are assigned to the photodetachment of $HCCCN^-$ and $CCHCN^-$, respectively. The individual vibrational transitions of band B are labeled 0, 1, and 2. The spectral peak energies and photoelectron anisotropy parameters are summarized in Table 1.

TABLE 1: Photoelectron Band Energies and Anisotropy Parameter (β) Values Determined from the $CCHCN^-$/$HCCCN^-$ Photoelectron Images Shown in Figure 1[a]

band	wavelength (nm)	eBE (eV)	eKE (eV)	β
A	532	1.04	1.29	0.32 ± 0.04
	355	1.04	2.45	0.06 ± 0.04
B(0)	532	1.85	0.48	-0.40 ± 0.04
	355	1.83	1.66	-0.47 ± 0.15
B(1)	532	1.97	0.36	-0.42 ± 0.04
	355	1.94	1.55	-0.30 ± 0.20
B(2)	532	2.06	0.27	-0.32 ± 0.08
	355	2.03	1.46	-0.10 ± 0.13

[a] The anisotropies are average values; uncertainties are standard deviations.

equilibrium geometries of the cyanovinylidene anion and the corresponding neutral. The same approximation breaks down in the case of $HCCCN^-$, because of the vastly different equilibrium geometries of the anion and the neutral.

4. Experimental Results and Spectroscopic Assignments

The 532 and 355 nm photoelectron images and the corresponding photoelectron spectra for the $m/z = 51$ anions ($CCHCN^-$ and $HCCCN^-$) are shown in Figure 1. While the 532 nm data were included in our preliminary report,[15] the 355 nm results are presented here for the first time. Both images show two distinct features. In the 532 nm image, the outer band, A, peaks in the direction parallel to the laser polarization axis, while the inner feature, B, consisting of several well-resolved vibrational bands, peaks in the perpendicular direction. In the 355 nm image, the bands are shifted to higher eKE and, owing to the decrease in absolute energy resolution with increasing eKE, the vibrational bands comprising feature B are less resolved, compared to the 532 nm image.

The 532 and 355 nm photoelectron spectra are plotted in Figure 1 versus electron binding energy (eBE). The two spectra are in excellent agreement. The first three vibrational peaks of band B are assigned labels 0, 1, and 2, appearing in parentheses in the text and Table 1. The origin transition, B(0), is centered at eBE = 1.85 eV in the 532 nm spectrum and 1.83 eV in the 355 nm spectrum. The origin of band B is therefore determined to be at eBE = 1.84 ± 0.01 eV. The origin transition corresponds to the most intense peak in the vibrational progression. Its energy, therefore, corresponds to both the adiabatic electron affinity of the neutral and the vertical detachment energy (VDE) of the anion.

The above experimentally determined value agrees with the VDE = 1.85 eV predicted at a high level of theory for the cyanovinylidene anion.[14] We therefore assign band B to the photodetachment of $CCHCN^-$. This assignment is further supported by the Franck−Condon analysis in section 5.2 below. We also note that cyanovinylidene anions were previously observed in the reaction of O^- with acrylonitrile,[21] but the photoelectron spectrum of $CCHCN^-$ had not been known until our recent preliminary report[15] and is discussed here in detail for the first time.

The broad and structureless band A in Figure 1 shows an onset at eBE $\approx$ 0.5 eV and a maximum at 1.04 ± 0.05 eV. The latter corresponds to the vertical detachment energy of the anion. Since band A is lower in energy relative to band B, it is attributed to a different species. With support from the theoretical predictions in section 5, band A is assigned to the cyanoacetylene form of the anion, $HCCCN^-$.[15]

The energetics and the anisotropy parameters determined for the different spectral features are summarized in Table 1. At 532 nm, band A ($HCCCN^-$) shows a slightly parallel PAD with a β value of 0.32, while the vibrational features of band B ($CCHCN^-$) are perpendicular in character, with β values of approximately −0.40. Larger uncertainties are associated with the 355 nm β values due to the poorer signal-to-noise of the data, but the opposite signs of β for bands A and B are also discerned in the 355 nm results.

5. Discussion

5.1. Cyanovinylidene and Cyanoacetylene Structures and Energetics. Figure 2 shows the geometries of $CCHCN^-$ (bottom left), $HCCCN^-$ (bottom right), the CCHCN singlet (S) and triplet (T) states (middle and top left, respectively), and the ground (singlet) state of HCCCN (middle right). In addition, the transition state (TS) for cyanovinylidene → cyanoacetylene rearrangement is also shown (top right inset). All structures were optimized at the B3LYP/aug-cc-pVDZ level of density-functional theory (DFT). MP2/aug-cc-pVDZ calculations give similar structures. The geometry of cyanovinylidene (S) shown in Figure 2 is very similar to the structure determined using a combination of the Brueckner coupled cluster and DFT methods, BCCSD(T)/cc-pVTZ and B3LYP/aug-cc-pVTZ.[20] The cyanoacetylene anion structure is qualitatively similar to that predicted at the CCSD(T)/aug-cc-pVDZ level of theory,[14] although some of the bond angles are not reproduced very well by the DFT.

The relative energies for the different cyanovinylidene and cyanoacetylene structures obtained using various levels of theory are summarized in Table 2. Figure 3 shows an energy diagram, which is based primarily on the DFT results, supplemented by the relevant experimentally determined values (this work) and the G3(MP2) and CCSD(T) results of Sommerfeld and Knecht.[14] The diagram is intended as a survey of the relevant structures and energy levels. The deficiencies of the inexpensive DFT calculations should not mask the important qualitative features of the potential energy landscape, as the quantitative details can be adjusted wherever higher-level ab initio results are available.[8,14,20]

All energies in Table 2 and Figure 3 are in electronvolts relative to the HCCCN (S) ground state. The black and red lines

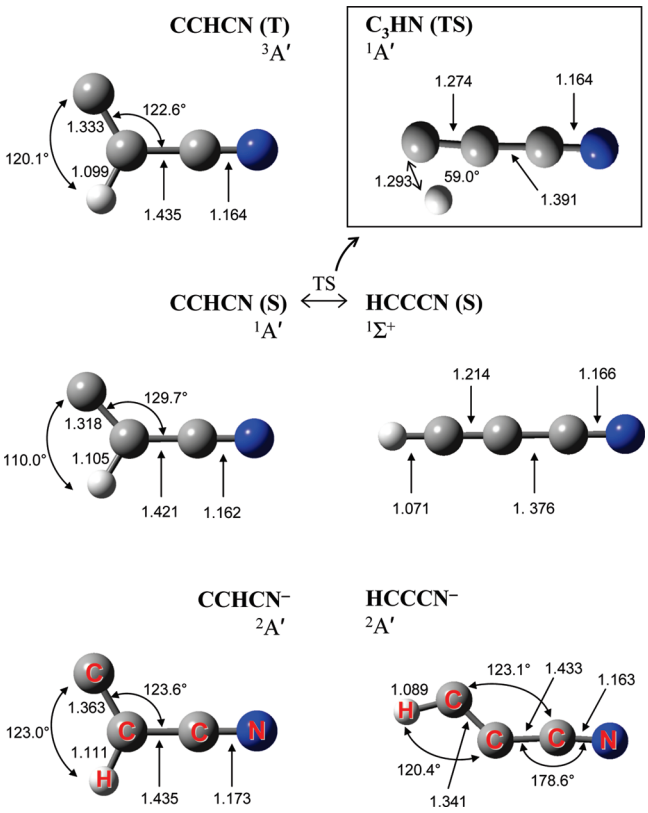

Figure 2. Optimized structures of $CCHCN^-$ and $HCCCN^-$, CCHCN and HCCCN ground state singlets (S), and the excited state triplet (T) of CCHCN. The inset in the top right shows the predicted geometry of the transition state (TS) on the singlet potential energy surface for the cyanovinylidene → cyanoacetylene rearrangement. All structures shown are from the B3LYP/-cc-pVDZ calculations. The bond lengths are indicated in Angstroms. The corresponding state energies are summarized in Table 2.

in Figure 3 correspond to the neutral and anion structures, respectively. As expected, cyanovinylidene corresponds to a shallow local minimum on the neutral potential energy surface for the 1,2-H atom shift to the more stable cyanoacetylene structure. According to the B3LYP/aug-cc-pVDZ prediction, the transition state (TS) for the CCHCN (S) → HCCCN (S) rearrangement lies only 0.02 eV above the CCHCN minimum. Although the rearrangement barrier is expected to be small, it is evident that its height is underestimated by the DFT calculation, as both MP2 (Table 2) and CCSD(T) (Table 2 and ref 8) predict barrier heights of about 0.09 eV (2.2 kcal/mol).[8]

On the anion surface, the two isomers are separated by a large potential barrier, corresponding to the anionic transition state (TS^-). The DFT calculations indicate that the cyanoacetylene anion is more stable than the cyanovinylidene anion, contrasting the relative energetics of unsubstituted acetylene and vinylidene. The same calculations predict an adiabatic electron affinity of 0.46 eV for neutral cyanoacetylene and a VDE of 1.40 eV for the corresponding anion. The CCSD(T)/aug-cc-pVDZ calculations have indicated an adiabatic electron affinity of 0.05 eV and a VDE of 1.25 eV.[14] Comparing these results, we are inclined to believe that the DFT exaggerates the stability of $HCCCN^-$ relative to HCCCN, as well as, probably, relative to $CCHCN^-$. However, the overall features of the energy diagram in Figure 3, especially the existence of stable $HCCCN^-$, are not in doubt.[14,15]

The adiabatic electron affinity of HCCCN cannot be determined from the photoelectron spectra of $HCCCN^-$, since the corresponding band in Figure 1, band A, shows no identifiable origin. This is due to the large geometry difference between the equilibrium $HCCCN^-$ and HCCCN structures (Figure 2). However, the above theoretical values for the anion VDE compare reasonably well with the experimental result of 1.04 ± 0.05 eV, especially considering that the electronic structures of weakly bound anions are notoriously difficult to model theoretically.

The purple dashed lines in Figure 3 correspond to the $CCHCN^-$, *trans*-$HCCCN^-$, and *cis*-$HCCCN^-$ anion structures obtained from acrylonitrile via the vertical 1,1-H_2^+, *trans*-1,2-H_2^+, and *cis*-1,2-H_2^+ abstraction processes (so labeled in the figure), respectively. These structures, referred to as the vertical abstraction geometries, are derived from the equilibrium structure of acrylonitrile with the two indicated hydrogen atoms, plus a charge, removed without changes to other bond lengths or angles (see also Figure 1 in ref 15). Unstable with respect to geometry relaxation, the vertical abstraction structures correspond to the sudden limit of anion formation by H_2^+ abstraction from acrylonitrile. Although the sudden approximation is admittedly crude, it provides useful guides for estimating the nascent $CCHCN^-$ and $^-$ excitations.

The *trans*-1,2-H_2^+ vertical abstraction geometry of $HCCCN^-$ is rather similar to the equilibrium *trans* structure of $HCCCN^-$. This structural similarity is the key to the formation of the $HCCCN^-$ anion.[15] The vertical *cis*-1,2-H_2^+ abstraction process, on the other hand, yields the anion in the initial *cis* configuration. The DFT calculations did not locate a local $HCCCN^-$ minimum corresponding to a *cis* geometry. That is, while *cis*-$HCCCN^-$ is vertically stable with respect to electron detachment, we expect it to be unstable with respect to rearrangement to the *trans* form of the anion. Therefore, regardless of the mechanistic details, the 1,2-H_2^+ abstraction reaction should ultimately yield $HCCCN^-$ anions in their equilibrium *trans* configuration.

On the other hand, the nascent energies of $CCHCN^-$ and $HCCCN^-$ formed by vertical 1,1-H_2^+ and 1,2-H_2^+ abstraction from acrylonitrile are estimated to be significantly lower than the barrier separating the cyanovinylidene and cyanoacetylene minimum energy forms of the anion (Figure 3). We therefore predict that the $CCHCN^-$ and $HCCCN^-$ products of the O^- + H_2CCHCN reaction do not interconvert into one another.

5.2. Analysis of the $CCHCN^-$ Spectrum. Calculations (summarized in Table 2) predict the adiabatic electron binding energy of the cyanovinylidene anion, $CCHCN^-$, is in the range 1.65−2.06 eV. These predictions are in good agreement with the origin of band B in the photoelectron spectra in Figure 1 observed at 1.84 ± 0.01 eV. A comparison with the previously reported spectra of other substituted vinylidenes provides further support for this band's assignment. Table 3 gives a summary of the eBEs and photoelectron anisotropy parameters determined for the anions of vinylidene, fluorovinylidene, vinylvinylidene, and cyanovinylidene. Since the cyano group acts as a pseudohalogen, we might expect the electron affinity of singlet cyanovinylidene (1.84 ± 0.01 eV) to be comparable to that of the X^1A' state of fluorovinylidene. The latter was determined to be 1.718 eV.[9]

Since no higher-energy bands are observed in the photoelectron spectra in Figure 1, the first excited state of cyanovinylidene (a $^3A'$) must lie outside the experiment's energy range. The 3.49 eV energy of 355 nm photons combined with the 1.84 eV electron affinity of the ground singlet state gives a 1.65 eV lower bound for the singlet−triplet splitting. The theoretical results summarized in Table 2 support this conclusion.

TABLE 2: Calculated Energies (eV) of Various Cyanovinylidene and Cyanoacetylene Neutral and Anion Structures Determined at Different Levels of Theory[a]

structure	electronic state	B3LYP aug-cc-pVDZ	MP2 aug-cc-pVDZ	CCSD(T) 6-311++G**	CCSD(T) aug-cc-pVDZ
$CCHCN^-$	$^2A'$	−0.04	0.72	0.46	n/a
CCHCN (S)	$^1A'$	2.03	2.37	2.15	n/a
CCHCN (T)	$^3A'$	3.90	4.78	3.90	n/a
TS	$^1A'$	2.05	2.28	2.23	n/a
HCCCN (S)	$^1\Sigma_g$	**0.00**	0.00	0.00	0.00
HCCCN (T)	$^3A''$	3.60	n/a	n/a	n/a
$HCCCN^-$	$^2A'$	−0.46	0.22	n/a	−0.05
TS^-	$^2A'$	2.08	n/a	n/a	n/a
source		this work	this work	this work	ref 14

[a] The corresponding structures are shown in Figure 2, with the exception of HCCCN (T) and TS^-.

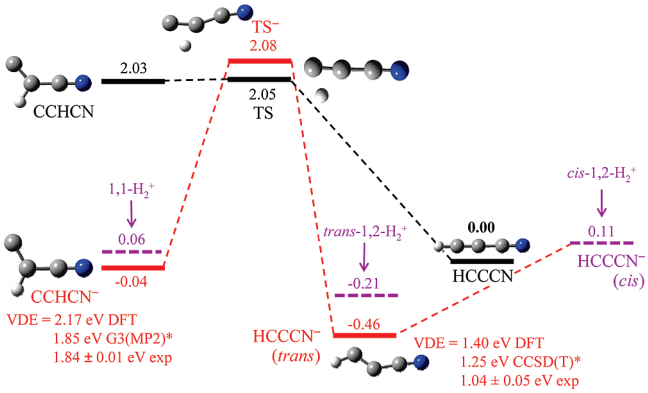

Figure 3. Schematic diagram (not to scale) showing the relative energies of different cyanovinylidene and cyanoacetylene anion and neutral structures. Geometric details of most structures are found in Figure 2. The diagram is based on the results of the B3LYP/aug-cc-pVDZ calculations, supplemented by the relevant experimentally determined values (marked "exp") and the G3(MP2) and CCSD(T)/aug-cc-pVDZ results from ref 14 (marked with asterisks). The energies are indicated in electronvolts, relative to the ground state of HCCCN. The black and red lines correspond to the neutral and anion structures, respectively. The purple dashed lines correspond to the $CCHCN^-$, *trans*-$HCCCN^-$, and *cis*-$HCCCN^-$ anion structures obtained from acrylonitrile via the vertical (sudden) 1,1-H_2^+, *trans*-1,2-H_2^+, and *cis*-1,2-H_2^+ abstraction processes, respectively.

The features of band B in Figure 1 support its assignment to the cyanovinylidene anion. The optimized $CCHCN^-$ and CCHCN (S) structures shown in Figure 2 are not considerably different. In fact, the optimized geometries of both singlet and triplet cyanovinylidene resemble the corresponding anion structure. The most noticeable change upon anion photodetachment to the singlet occurs in the CCH bond angle, which decreases by 13°. The predicted structural similarity is consistent with the sharp onset of band B and the appearance of a defined vibrational progression. These properties contrast with the broad and unstructured band A, which corresponds to a large geometry change expected in the photodetachment of $HCCCN^-$.

The predicted similarity of the optimized $CCHCN^-$ and CCHCN (S) structures makes this system suitable for Franck−Condon simulations in the parallel-mode approximation. We used this approach, as described in section 3, in conjunction with the results of the B3LYP/aug-cc-pVDZ calculations for $CCHCN^-$ and CCHCN (S) to simulate the photoelectron spectrum of the cyanovinylidene anion. The simulated stick spectrum was convoluted with a Gaussian function to reproduce the observed peak widths and shifted to overlap the band origin in the experimental spectrum. The simulated spectrum is shown in Figure 4, where it is compared to the 532 nm experimental spectrum (band B, reproduced from Figure 1).

The two spectra are in good overall agreement, confirming the validity of the spectral assignment, although the intensities of the higher-order vibrational peaks are not well reproduced. As the simulated spectrum does not involve any fitting parameters, other than a shift of the transition's origin, an instrumental peak broadening factor, and a scaling factor for frequencies, an exact agreement cannot be expected. The discrepancies are most likely due to the use of the parallel mode approximation used instead of calculating the full multidimensional overlap integrals. Although the full Franck−Condon treatment would likely result in a better fit, our simulation procedure is adequate for assigning the vibrational progression of band B to the X^1A' state of cyanovinylidene.

The major progression in the simulated spectrum in Figure 4 corresponds to the calculated (unscaled) CCH bend frequency of 924 cm^{-1}. By comparing the optimized geometries in Figure 2, we see the CCH bond angle decreases noticeably upon electron detachment from $CCHCN^-$ to the X^1A' state of CCHCN. The average peak spacing in both the 355 and 532 nm spectra in Figure 1 is in agreement with the calculated frequency. All vibrational modes were included in the simulation, but only the CCH bend shows appreciable intensity in our spectrum.

The lifetimes of reactive intermediates can be estimated by line shape analysis. In the previous studies of vinylidenes,[2,9,11] this is done by first modeling the line shapes corresponding to the triplet state to determine the rotational temperature of the ions and then using the result to simulate the rotational profile for the singlet state. The remaining peak width, unaccounted for by the rotational contribution, is attributed to lifetime broadening. In the present experiment, the triplet state is not observed and the rotational temperature of the ions is not known. If we assume that the full width at half-maximum of the B(0) peak in the 532 nm photoelectron spectrum in Figure 1 (∼45 meV) is due to lifetime broadening, the lower limit for the lifetime of cyanovinylidene is estimated to be ∼30 fs.

This limit is consistent with the previous studies of vinylidene, which found lifetimes of 20−200 fs.[2] However, it does not take into account the instrumental response and the rotational envelope of the transitions. In the studies of other ions with similar energetics under similar experimental conditions, we found line widths of about 20−25 meV. As a very crude estimate, it can be assumed that a similar line shape accounts for the instrumental and rotational profiles of the $CCHCN^-$ transitions. The effect of lifetime broadening can then be estimated by deconvoluting a 25 meV wide line shape function from a 45 meV wide envelope of the B(0) transition. Using Gaussian line shape functions, this procedure yields a lifetime broadening of 35−40 meV, corresponding to a ∼35 fs lifetime—only slightly increased compared to the initial estimate.

TABLE 3: Electron Binding Energies and Photoelectron Anisotropies Observed in the Photodetachment of the Vinylidene, Fluorovinylidene, Vinylvinylidene, and Cyanovinylidene Anions

neutral molecule electronic state	wavelength (nm)	electron binding	parameter, β	source
		H_2CC		
X^1A_1	351.1	0.490	−0.51	
a^3B_2	351.1	2.555	+1.45	ref 2
b^3A_2	351.1	3.244	−0.5	
		HFCC		
X^1A'	351.1	1.718	n/a	ref 9
b^3A'	351.1	3.076	+1.1	
		C_4H_4		
X^1A'	351.1	0.914	−0.10	ref 10
a^3A'	351.1	3.038	+0.95	
		CCHCN		
X^1A'	355	1.83	−0.399	this work

We caution, however, that the rotational constants and temperatures can differ significantly for different ions, so this estimate is still only a lower limit for the lifetime of cyanovinylidene.

5.3. Photoelectron Angular Distributions. The photoelectron angular distributions may serve as additional indicators of the nature of the initial anion and final neutral electronic states. The PADs reflect the symmetry of the parent orbitals from which the electrons are ejected. Both $CCHCN^-$ and $HCCCN^-$ have planar equilibrium geometries, corresponding to the C_s symmetry point group and in both cases the highest-occupied molecular orbitals (HOMO) transform under the a′ irreducible representation. In general, parallel PADs are usually expected in the photodetachment from totally symmetric orbitals. Among the C_s point group examples, in the previous study of vinoxide, detachment from the a′ orbitals yielded parallel PADs ($\beta > 0$), while detachment from the a″ orbitals yielded perpendicular distributions ($\beta < 0$).[36] The same trend was recently demonstrated for the nitromethane anion.[37]

In the present work, the positive β values observed for band A (Table 1) are consistent with the above arguments, considering the a′ symmetry HOMO of $HCCCN^-$. However, the PADs for band B ($CCHCN^-$) are predominantly perpendicular in character ($\beta < 0$), even though the band is also assigned to electron detachment from the a′ symmetry HOMO. The apparent discrepancy is due to the low symmetry of the C_s point group, where two of the three orthogonal coordinate vectors transform as the nondegenerate representation a′. The limitation of the symmetry-based approach can be heightened to the extreme, if one considers an asymmetric molecule (C_1 point group), in which *all* orbitals transform under the same, nominally "totally symmetric" representation. Photodetachment transitions in such anions may still produce PADs of different characters and perpendicular ($\beta < 0$) transitions are not forbidden by any means, while the symmetry analysis becomes trivial and obsolete in such a case. Hence, the strict symmetry-based PAD analysis, proven to be quite powerful for C_{2v} and higher-symmetry species,[38−40] is less useful in systems of reduced symmetry. Even though its utility has been demonstrated in some C_s symmetry cases,[36,37] the present contradictory examples of $CCHCN^-$ and $HCCCN^-$ emphasize the need for other approaches.

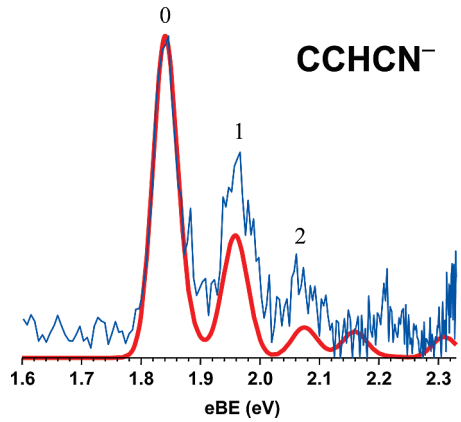

Figure 4. Bold red line: simulated photoelectron spectrum of $CCHCN^-$. Thin blue line: the corresponding experimental spectrum (band B at 532 nm, reproduced from Figure 1). The simulated spectrum was calculated using the B3LYP/aug-cc-pVDZ molecular parameters for $CCHCN^-$ and CCHCN (S). The stick spectrum, calculated using the parallel mode approximation, as described in the text, was shifted to match the experimental band origin and convoluted with a Gaussian function to reproduce the experimental spectrum shown in the figure.

The perpendicular PADs observed for $CCHCN^-$ (band B, Table 1) are not surprising, if we compare the reported β values with those obtained for other vinylidenes. Table 3 lists the anisotropy parameters reported for the photodetachment of the vinylidene,[2] fluorovinylidene,[9] and vinylvinylidene[10] anions, in comparison to cyanovinylidene. In all available cases, photodetachment to the ground neutral state displays perpendicular PADs ($\beta < 0$). Both fluorovinylidene and vinylvinylidene have C_s symmetry structures with a′ symmetry HOMOs, consistent with the present case of cyanovinylidene. The vinylidene anion has C_{2v} symmetry, and the lowest photodetachment transition originates from a b_2 orbital. Group symmetry analysis for the C_{2v} point group correctly predicts the perpendicular nature of the PAD in this case.[38]

Finally, for *all* vinylidene anions in Table 3, the HOMOs are qualitatively described as carbon π*2p orbitals in the plane of the molecule, which are similar in character to the π_g* (d_{xy}-like) HOMO of O_2^-. The photodetachment of superoxide is known to yield predominantly perpendicular angular distributions,[41−43] lending additional support for the interpretation of the present cyanovinylidene results.

6. Conclusions

The cyanoacetylene and cyanovinylidene anions are generated simultaneously via the competing 1,1-H_2^+ and 1,2-H_2^+ abstraction channels of O^- reaction with acrylonitrile. Via photodetachment, the two isomeric forms of the anion, separated by a large (∼2 eV) potential energy barrier, provide access to both the reactant and the product sides of the neutral cyanovinylidene → cyanoacetylene rearrangement reaction.

Using photoelectron imaging spectroscopy at 532 and 355 nm, the adiabatic electron affinity of cyanovinylidene (X^1A') is

determined to be 1.84 ± 0.01 eV, while the first excited state (a $^3A'$) lies at least 1.65 eV higher. Using electronic structure calculations, the equilibrium geometry of $CCHCN^-$ is predicted to be rather similar to that of neutral cyanovinylidene. The major vibrational progression in the $X^1A' \leftarrow X^2A'$ photoelectron spectrum of $CCHCN^-$ is attributed to the excitation of the CCH bending mode. The spectral features are reproduced reasonably well using a Franck−Condon simulation under the parallel-mode approximation, while a crude line shape analysis gives a lower bound for the cyanovinylidene rearrangement lifetime of ∼30−35 fs.

In contrast to unsubstituted acetylene, cyanoacetylene has a stable anionic state. The valence $HCCCN^-$ structure,[14] which had until recently eluded experimental detection,[15] is adiabatically weakly bound with respect to electron detachment[14] but has an experimentally determined vertical detachment energy of 1.04 ± 0.05 eV.

Acknowledgment. This research is supported by the National Science Foundation (grant CHE-0713880).

References and Notes

(1) Burnett, S. M.; Stevens, A. E.; Feigerle, C. S.; Lineberger, W. C. *Chem. Phys. Lett.* **1983**, *100*, 124.
(2) Ervin, K. M.; Ho, J.; Lineberger, W. C. *J. Chem. Phys.* **1989**, *91*, 5974.
(3) Carrington, T.; Hubbard, L. M.; Schaefer, H. F.; Miller, W. H. *J. Chem. Phys.* **1984**, *80*, 4347.
(4) Dykstra, C. E.; Schaefer, H. F. *J. Am. Chem. Soc.* **1978**, *100*, 1378.
(5) Conrad, M. P.; Schaefer, H. F. *J. Am. Chem. Soc.* **1978**, *100*, 7820.
(6) Osamura, Y.; Schaefer, H. F.; Gray, S. K.; Miller, W. H. *J. Am. Chem. Soc.* **1981**, *103*, 1904.
(7) Gallo, M. M.; Hamilton, T. P.; Schaefer, H. F. *J. Am. Chem. Soc.* **1990**, *112*, 8714.
(8) Hu, C. H.; Schaefer, H. F. *J. Phys. Chem.* **1993**, *97*, 10681.
(9) Gilles, M. K.; Lineberger, W. C.; Ervin, K. M. *J. Am. Chem. Soc.* **1993**, *115*, 1031.
(10) Gunion, R. F.; Koppel, H.; Leach, G. W.; Lineberger, W. C. *J. Chem. Phys.* **1995**, *103*, 1250.
(11) Gunion, R. F.; Lineberger, W. C. *J. Phys. Chem.* **1996**, *100*, 4395.
(12) Deleeuw, B. J.; Fermann, J. T.; Xie, Y. M.; Schaefer, H. F. *J. Am. Chem. Soc.* **1993**, *115*, 1039.
(13) Collins, C. L.; Hu, C. H.; Yamaguchi, Y.; Schaefer, H. F. *Isr. J. Chem.* **1993**, *33*, 317.
(14) Sommerfeld, T.; Knecht, S. *Eur. Phys. J. D* **2005**, *35*, 207.
(15) Goebbert, D. J.; Khuseynov, D.; Sanov, A. *J. Chem. Phys.* **2009**, *131*, 161102.
(16) Graupner, K.; Merrigan, T. L.; Field, T. A.; Youngs, T. G. A.; Marr, P. C. *New J. Phys.* **2006**, *8*, 117.
(17) Kolos, R.; Gronowski, M.; Botschwina, P. *J. Chem. Phys.* **2008**, *128*, 154305.
(18) Thaddeus, P.; Gottlieb, C. A.; Gupta, H.; Brunken, S.; McCarthy, M. C.; Agundez, M.; Guelin, M.; Cernicharo, J. *Astophys. J.* **2008**, *677*, 1132.
(19) Botschwina, P.; Oswald, R. *J. Chem. Phys.* **2008**, *129*, 044305.
(20) Kolos, R.; Gronowski, M.; Dobrowolski, J. C. *Astophys. J.* **2009**, *701*, 488.
(21) Dawson, J. H. J.; Nibbering, N. M. M. *Int. J. Mass Spectrom. Ion Physics* **1980**, *33*, 3.
(22) Heni, M.; Illenberger, E. *Int. J. Mass Spectrom. Ion Processes* **1986**, *73*, 127.
(23) Duschinsky, F. *Acta Physicochim. URSS* **1937**, *7*, 551.
(24) Velarde, L.; Habteyes, T.; Sanov, A. *J. Chem. Phys.* **2006**, *125*, 114303.
(25) Dawson, J. H. J.; Jennings, K. R. *Faraday Trans. II* **1976**, *72*, 700.
(26) Eppink, A.; Parker, D. H. *Rev. Sci. Instrum.* **1997**, *68*, 3477.
(27) Chandler, D. W.; Houston, P. L. *J. Chem. Phys.* **1987**, *87*, 1445.
(28) Dribinski, V.; Ossadtchi, A.; Mandelshtam, V. A.; Reisler, H. *Rev. Sci. Instrum.* **2002**, *73*, 2634.
(29) Cavanagh, S. J.; Gibson, S. T.; Gale, M. N.; Dedman, C. J.; Roberts, E. H.; Lewis, B. R. *Phys. Rev. A* **2007**, *76*, 052708.
(30) Cooper, J.; Zare, R. N. *J. Chem. Phys.* **1968**, *48*, 942.
(31) Cooper, J.; Zare, R. N. *J. Chem. Phys.* **1968**, *49*, 4252.
(32) Frisch, M. J. et al. *Gaussian 03*, revision C.02; Gaussian, Inc.: Wallingford, CT, 2004.
(33) Kohn, D. W.; Robles, E. S. J.; Logan, C. F.; Chen, P. *J. Phys. Chem.* **1993**, *97*, 4936.
(34) Sharp, T. E.; Rosenstock, H. M. *J. Chem. Phys.* **1964**, *41*, 3453.
(35) Ervin, K. M.; Ramond, T. M.; Davico, G. E.; Schwartz, R. L.; Casey, S. M.; Lineberger, W. C. *J. Phys. Chem. A* **2001**, *105*, 10822.
(36) Bowen, M. S.; Continetti, R. E. *J. Phys. Chem. A* **2004**, *108*, 7827.
(37) Goebbert, D. J.; Pichugin, K.; Sanov, A. *J. Chem. Phys.* **2009**, *131*, 164308.
(38) Surber, E.; Mabbs, R.; Sanov, A. *J. Phys. Chem. A* **2003**, *107*, 8215.
(39) Sanov, A.; Mabbs, R. *Int. Rev. Phys. Chem.* **2008**, *27*, 53.
(40) Mabbs, R.; Grumbling, E. R.; Pichugin, K.; Sanov, A. *Chem. Soc. Rev.* **2009**, *38*, 2169.
(41) Akin, F. A.; Schirra, L. K.; Sanov, A. *J. Phys. Chem. A* **2006**, *110*, 8031.
(42) Goebbert, D. J.; Sanov, A. *J. Chem. Phys.* **2009**, *131*, 104308.
(43) Oana, C. M.; Krylov, A. I. *J. Chem. Phys.* **2009**, *131*, 124114.

JP9106102